ELSEVIER

Journal of Nuclear Materials 289 (2001) 16–22

journal of nuclear materials

www.elsevier.nl/locate/jnucmat

Computational analysis of creep fracture deformation in SiC/SiC composites

H. Serizawa [a,*], M. Ando [b], C.A. Lewinsohn [c], H. Murakawa [a]

[a] *Joining and Welding Research Institute, Osaka University, 11-1 Mihogaoka, Ibaraki, Osaka 567-0047, Japan*
[b] *Graduate School of Engineering, Osaka University, 2-1 Yamada-oka, Suita, Osaka 565-0871, Japan*
[c] *Pacific Northwest National Laboratory, MSIN:P8-15, P.O. Box 999, Richland, WA 99352, USA*

Abstract

Creep fracture deformation in SiC/SiC composites was analyzed using a new computer simulation method with time-dependent interface elements. The simulation method was used to describe the crack growth deformation in SiC/SiC composite under four-point bending of single-edge-notched beam bend-bars. Two methods were used to simulate the crack growth due to fiber creep. In one method, the creep property was introduced into the interface elements by the general method of FEM analysis. In the second method, a new technique making the best use of the potential function was used. The stage-II steady-state creep deformation was simulated by both methods, and the stage-III crack growth and the transition from stage-II to stage-III could be simulated by only the new method. Additionally, the stage-I was simulated by the new method. The new method has the potential to completely simulate creep fracture deformation in SiC/SiC composite due to fiber creep.

1. Introduction

Silicon carbide fiber-reinforced silicon carbide composites (SiC/SiC) are promising candidates as high flux component materials, due to their potential of low-activation, low-afterheat and excellent high-temperature properties [1–4]. For safe design of fusion structures, it is very important to reliably estimate the creep fracture deformation of materials.

For SiC/SiC composites, matrix cracking precedes fiber failure. Following matrix cracking, intact fibers bridge the cracks and impose closure tractions behind the crack tip that reduce the driving force for further cracking (crack-tip shielding). Fracture is governed by creep of the bridging fibers, which relaxes the bridging tractions causing the stress intensity at the crack tip to increase. Then the creep fracture deformation in SiC/SiC composites has been studied as the microstructural fracture behavior, namely the formation and propagation of cracks in the fiber bridging zone, and it has been statically analyzed previously [5–7]. It is reported that crack growth of SiC/SiC composites in inert environments (slow crack growth) is controlled by the creep rate of the bridging fibers [6]. The macroscopic and dynamic deformations, however, have not been sufficiently described.

To more completely describe deformation and fracture behavior, a new and simple computer simulation method [8,9] was developed. The method treats the fracture phenomena as the formation of new surface during the crack propagation. Based on the fact that surface energy must be supplied for the formation of new surface, a potential function representing the density of surface energy is introduced to the finite element method (FEM) using proposed interface elements. In this research, a new, time-dependent interface element was developed to incorporate the creep behavior of fibers into FEM. This technique was then used to analyze creep fracture deformation in SiC/SiC composites.

2. Interface potential

For the case of ordinary crack propagation problems, a method using interface elements has been

* Corresponding author. Tel.: +81-6 6879 8665; fax: +81-6 6879 8689.
E-mail address: serizawa@jwri.osaka-u.ac.jp (H. Serizawa).

0022-3115/01/$ - see front matter
PII: S0022-3115(00)00677-2

proposed [8,9]. In this method, the formation and propagation of a crack are governed by the interface potential energy function. The requirements of the interface potential energy function are:

1. it involves the surface energy necessary to form new surface;
2. it is a continuous function of crack opening displacement, δ.

Among many functions satisfying these requirements, a Lennard–Jones type potential [10] may be employed where the potential energy $\phi(\delta)$ is defined by the following equation:

$$\phi(\delta) \equiv 2\gamma \cdot \left\{ \left(\frac{r_0}{r_0 + \delta} \right)^{2n} - 2 \cdot \left(\frac{r_0}{r_0 + \delta} \right)^{n} \right\}, \quad (1)$$

where δ is the crack opening displacement and γ, n and r_0 are material constants. In particular, 2γ is the surface energy per unit area. This form of the Lennard–Jones type potential function, has been used to simulate peeling tests of metal plating on ABS resin. Since the agreement between the simulations and experimental results were good [8], the same potential function was used in this study.

The derivative of ϕ with respect to the crack opening δ , as shown in the following equation, gives the bonding strength per unit area of the crack surface

$$\sigma = \frac{\partial \phi}{\partial \delta} = \frac{4\gamma \cdot n}{r_0} \cdot \left\{ \left(\frac{r_0}{r_0 + \delta} \right)^{n+1} - \left(\frac{r_0}{r_0 + \delta} \right)^{2n+1} \right\}. \quad (2)$$

3. Modeling method

Fig. 1 shows a schematic illustration of the bridging zone. In this method, the bridging zone is analyzed macroscopically, not microscopically. One interface element is assumed to represent many fibers and the matrix in the bridging zone. The properties of the interface between fiber and matrix are assumed to be invariant with respect to time or displacement, hence they are not explicitly included in the model. In other words, effective matrix properties are used to incorporate both the true matrix and the interface. Away from the cracked region, the composite is described by ordinary FEM elements.

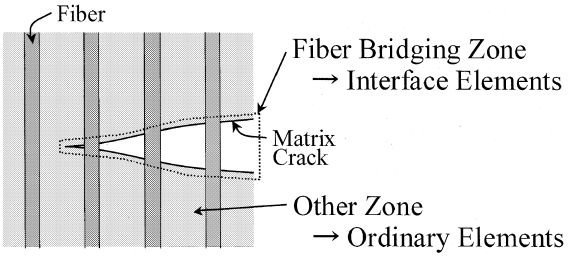

Fig. 1. Schematic illustration of bridging zone in composites.

Summation was used to characterize both fibers and matrices by one interface element. The interface potential $\phi(\delta)$ becomes:

$$\phi \equiv \phi_{\mathrm{f}} + \phi_{\mathrm{m}}, \quad (3)$$

$$\phi_{\mathrm{f}} \equiv 2\gamma_{\mathrm{f}} \cdot \left\{ \left(\frac{r_{\mathrm{f0}}}{r_{\mathrm{f0}} + \delta} \right)^{2n} - 2 \cdot \left(\frac{r_{\mathrm{f0}}}{r_{\mathrm{f0}} + \delta} \right)^{n} \right\}, \quad (4)$$

$$\phi_{\mathrm{m}} \equiv 2\gamma_{\mathrm{m}} \cdot \left\{ \left(\frac{r_{\mathrm{m0}}}{r_{\mathrm{m0}} + \delta} \right)^{2n} - 2 \cdot \left(\frac{r_{\mathrm{m0}}}{r_{\mathrm{m0}} + \delta} \right)^{n} \right\}, \quad (5)$$

where subscripts of f and m indicate fiber and matrix, respectively. Only ϕ_{f} was assumed to have a time dependency due to the creep effect of fiber. The effect of fiber creep was introduced by two methods: (1) the general method of FEM analysis with integral creep properties, and (2) a new method making the best use of a potential function.

4. Theoretical formulation

4.1. General method of FEM analysis

In the general method of FEM analysis for creep deformation, total strain can be divided into elastic strain, plastic strain, creep strain and possibly other strains (e.g., thermal strain). Typically, due to the brittleness of SiC/SiC composites, their deformation may be limited to elastic and creep deformation. The strain of ordinary elements in FEM is equal to the displacement in the interface element. For a fiber element, the displacement, δ, can be divided into an elastic displacement, δ^{e}, and a creep displacement, δ^{c}

$$\delta \equiv \delta^{\mathrm{e}} + \delta^{\mathrm{c}}. \quad (6)$$

According to the primary creep laws, the creep displacement δ^{c} is written by the following equation [11]:

$$\delta^{\mathrm{c}} \equiv A \cdot \sigma^{m} \cdot t^{p}, \quad (7)$$

where A, σ, m, p and t are constants describing the structure of the deformation, the applied stress of the interface element, the stress exponent, the creep time exponent and the creep time, respectively. Especially, for steady-state creep, p becomes to 1 and the creep displacement δ^{c} follows the classical Dorn formalism [12]

$$\delta^{\mathrm{c}} \equiv A \cdot \sigma^{m} \cdot t \quad (8)$$

On the other hand, in the case of the elastic displacement δ^{e}, the following equation must be satisfied at any time according to Eq. (4)

$$\phi_{\mathrm{f}}(\delta^{\mathrm{e}}) \equiv 2\gamma_{\mathrm{f}} \cdot \left\{ \left(\frac{r_{\mathrm{f0}}}{r_{\mathrm{f0}} + \delta^{\mathrm{e}}} \right)^{2n} - 2 \cdot \left(\frac{r_{\mathrm{f0}}}{r_{\mathrm{f0}} + \delta^{\mathrm{e}}} \right)^{n} \right\}, \qquad (9)$$

where the elastic displacement δ^{e} is obtained from the total displacement δ by Eq. (6). Then, since any creep deformation was not taken into account, the interface potential of the matrix $\phi_{\mathrm{m}}(\delta)$ becomes Eq. (5), where the displacement δ is the total displacement. In this general method, load vector and stiffness matrix for FEM can be obtained by the same process described in [8], so this is omitted.

4.2. A new method

In Eq. (4), there are three material constants, which are γ_{f}, r_{f0} and n. Among these constants, only r_{f0} has the same dimension as the total displacement δ. As written in the previous section, in general, the displacement δ is controlled by Eq. (7) during creep. In this research, to make the best use of the potential function, the parameter r_{f0} was assumed to be time dependent, and the increment of r_{f0} was defined by the following equation:

$$\Delta r_{\mathrm{f0}} = B \cdot \sigma^{m} \cdot t^{p}, \qquad (10)$$

where B is a constant, and the other parameters are the same as those in Eq. (7). The increment of r_{f0} for steady-state creep was also defined by the following equation similar to the previous section:

$$\Delta r_{\mathrm{f0}} = B \cdot \sigma^{m} \cdot t. \qquad (11)$$

Thus the interface potential energy of the fiber ϕ_{f} becomes a function of both opening displacement δ and time t, and is written as $\phi_{\mathrm{f}}(\delta, t)$. The total interface potential energy is also described as $\phi(\delta, t)$ while the interface potential energy of matrix ϕ_{m} is a function of only the opening displacement.

On the other hand, although balanced equations of the new method are the same as the equations of the general method [8], load vector and stiffness matrix are different. So these should be introduced. The time-dependent interface potential energy $\phi(\delta, t)$ is given by Eq. (12).

$$U_S^{\mathrm{e}}\left(u_0^{\mathrm{e}}, t\right) = \int \phi(\delta, t) \cdot \mathrm{d}S^{\mathrm{e}}, \qquad (12)$$

where U_S^{e} and u_0^{e} show interface potential energy of one element and nodal displacement. In Eq. (13), $U_S^{\mathrm{e}}(u_0^{\mathrm{e}} + \Delta u_0^{\mathrm{e}}, t + \Delta t)$ is transformed with Taylor's expansion about Δu_0^{e} and Δt

$$\begin{aligned} U_S^{\mathrm{e}}\left(u_0^{\mathrm{e}} + \Delta u_0^{\mathrm{e}}, t + \Delta t\right) &= \int \phi(\delta + \Delta\delta, t + \Delta t) \cdot \mathrm{d}S^{\mathrm{e}} \\ &= \int \phi \cdot \mathrm{d}S^{\mathrm{e}} \\ &\quad + \int \left(\frac{\partial \phi}{\partial \delta} \cdot \left\{ \frac{\partial \delta}{\partial u_0^{\mathrm{e}}} \right\}^{\mathrm{T}} + \frac{\partial^2 \phi}{\partial \delta \partial t} \cdot \left\{ \frac{\partial \delta}{\partial u_0^{\mathrm{e}}} \right\}^{\mathrm{T}} \cdot \Delta t \right) \\ &\quad \cdot \left\{ \Delta u_0^{\mathrm{e}} \right\} \cdot \mathrm{d}S^{\mathrm{e}} + \frac{1}{2} \cdot \int \left(\frac{\partial^2 \phi}{\partial \delta^2} + \frac{\partial^3 \phi}{\partial \delta^2 \partial t} \cdot \Delta t \right) \cdot \left\{ \Delta u_0^{\mathrm{e}} \right\}^{\mathrm{T}} \\ &\quad \cdot \left\{ \frac{\partial \delta}{\partial u_0^{\mathrm{e}}} \right\} \cdot \left\{ \frac{\partial \delta}{\partial u_0^{\mathrm{e}}} \right\}^{\mathrm{T}} \cdot \left\{ \Delta u_0^{\mathrm{e}} \right\} \cdot \mathrm{d}S^{\mathrm{e}} + \mathrm{H.O.T.} \end{aligned} \qquad (13)$$

First- and second-order terms about increment of nodal displacement Δu_0^{e} are arranged to these equations

$$\begin{aligned} &\int \left(\frac{\partial \phi}{\partial \delta} \cdot \left\{ \frac{\partial \delta}{\partial u_0^{\mathrm{e}}} \right\}^{\mathrm{T}} + \frac{\partial^2 \phi}{\partial \delta \partial t} \cdot \left\{ \frac{\partial \delta}{\partial u_0^{\mathrm{e}}} \right\}^{\mathrm{T}} \cdot \Delta t \right) \cdot \left\{ \Delta u_0^{\mathrm{e}} \right\} \cdot \mathrm{d}S^{\mathrm{e}} \\ &\quad = -\{f\}^{\mathrm{T}} \cdot \left\{ \Delta u_0^{\mathrm{e}} \right\}, \end{aligned} \qquad (14)$$

$$\begin{aligned} &\frac{1}{2} \cdot \int \left(\frac{\partial^2 \phi}{\partial \delta^2} + \frac{\partial^3 \phi}{\partial \delta^2 \partial t} \cdot \Delta t \right) \cdot \left\{ \Delta u_0^{\mathrm{e}} \right\}^{\mathrm{T}} \cdot \left\{ \frac{\partial \delta}{\partial u_0^{\mathrm{e}}} \right\} \cdot \left\{ \frac{\partial \delta}{\partial u_0^{\mathrm{e}}} \right\}^{\mathrm{T}} \\ &\quad \cdot \left\{ \Delta u_0^{\mathrm{e}} \right\} \cdot \mathrm{d}S^{\mathrm{e}} = \frac{1}{2} \cdot \left\{ \Delta u_0^{\mathrm{e}} \right\}^{\mathrm{T}} \cdot [K] \cdot \left\{ \Delta u_0^{\mathrm{e}} \right\}. \end{aligned} \qquad (15)$$

Load vector $\{f\}$ and stiffness matrix $[K]$ in time-dependent interface element are as coefficients of first- and second-order terms. That is,

$$\{f\} = -\int \left(\frac{\partial \phi}{\partial \delta} \cdot \left\{ \frac{\partial \delta}{\partial u_0^{\mathrm{e}}} \right\}^{\mathrm{T}} + \frac{\partial^2 \phi}{\partial \delta \partial t} \cdot \left\{ \frac{\partial \delta}{\partial u_0^{\mathrm{e}}} \right\}^{\mathrm{T}} \cdot \Delta t \right) \cdot \mathrm{d}S^{\mathrm{e}}, \qquad (16)$$

$$[K] = \int \left(\frac{\partial^2 \phi}{\partial \delta^2} + \frac{\partial^3 \phi}{\partial \delta^2 \partial t} \cdot \Delta t \right) \cdot \left\{ \frac{\partial \delta}{\partial u_0^{\mathrm{e}}} \right\}^{\mathrm{T}} \cdot \left\{ \frac{\partial \delta}{\partial u_0^{\mathrm{e}}} \right\} \cdot \mathrm{d}S^{\mathrm{e}}. \qquad (17)$$

5. FEM model

In this paper, the measured creep fracture deformation in SiC/SiC composites was obtained by loading single-edge-notched beam bend-bar specimens in four-point bending (Fig. 2(a)). The reinforcements of the composites were two-dimensional plain-weave Hi–Nicalon fiber mats stacked in the direction of thickness, and the matrices were deposited by chemical vapor infiltration. The applied load varied from 540 to 570 N in the temperature range from 1100°C to 1200°C. The size of the specimens was approximately $50 \times 5 \times 4$ mm^{-3}. The initial notch-to-depth ration was approximately 0.2. The

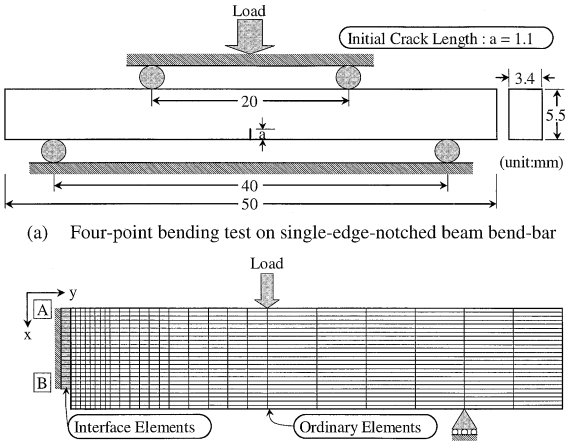

Fig. 2. Schematic illustration of bending test and FEM model for analysis.

atmosphere was gettered Ar (<20 ppm O_2). In these tests, the crack propagated from the tip of the notch in the direction parallel to the applied load. Experimental details were published elsewhere [6].

To examine the validity of the proposed method using the time-dependent interface element for the analysis of creep fracture deformation, the model shown in Fig. 2(b) was analyzed as a plain strain problem. Because of the symmetry of the problem, only the half of the specimen was used. The time-dependent interface elements were arranged along the crack propagation path. In this analysis, only the mode-I type crack propagation parallel to the y-axis in Fig. 2(b) was taken into account. The results of previous calculations [8] using the interface element described here, indicated that a value of 6 for the parameter n in Eq. (1) was appropriate for brittle fracture behavior such as the peeling test [8]. Therefore, in this analysis, the parameter n in Eqs. (4) and (5) was assumed to be (6).

6. Results and discussion

6.1. Steady-state creep deformation (stage-II)

Fig. 3 shows typical experimental results for the time-dependent crack growth in SiC/SiC composite reported, where the temperature was 1200°C and applied load was 556 N [6]. As an primarily analysis of creep deformation, although the clear stage-II slow crack growth (steady-state creep deformation) could not be observed in this figure, the proposed method with the time-dependent interface element was only compared with experimental result where the displacement was more than 0.06 mm. In this regime, the observed specimen behavior was almost steady-state and, hence, using a steady-state creep

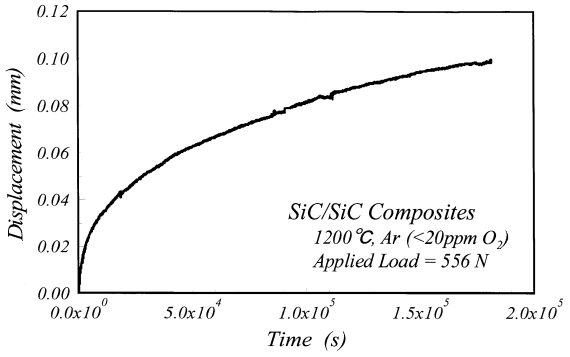

Fig. 3. Experimental displacement–time curve during time-dependent crack growth in SiC/SiC composite.

law to represent the interface elements (Eqs. (8) and (11)) was thought to be appropriate. Where the parameter m was assumed to be unity [13] since the test was performed at high-temperature.

Fig. 4 shows the experimental and calculated results using both the general and the new method. The parameters in Eqs. (4), (5), (8) and (11) were determined such that the calculated results fitted the quasi-steady state experimental creep result in the displacement range from 0.06 to 0.10 mm as best as possible. Therefore the parameters shown in Fig. 4 have no physical meaning. Nevertheless, the calculated results simulated the stage-II steady-state creep deformation. Furthermore, the results using the new method represented not only stage-II steady-state creep deformation but also stage-III crack growth. Although stage-III crack growth is not often observed under conditions relevant to fusion devices, it may occur under other conditions. Therefore, the new method was used to calculate crack growth under various applied loads.

The calculated results under various applied loads using the new method are shown in Fig. 5. The ends of curves indicate the fracture point of specimens. The

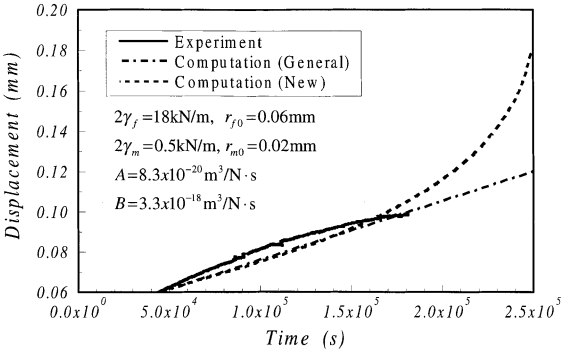

Fig. 4. Comparison between experiment and computation for time-dependent crack growth.

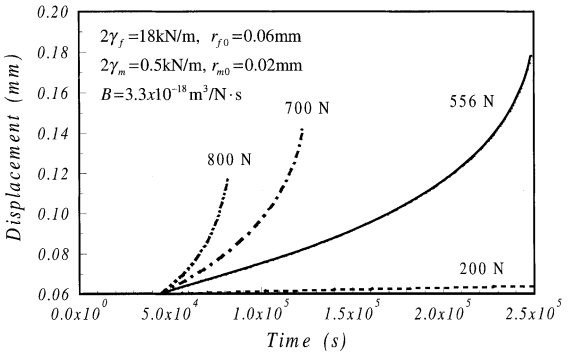

Fig. 5. Calculated displacement–time curves under various applied load for new method.

transition time from stage-II to stage-III decreased with increasing applied load, similar to the general creep deformation. Therefore the new method is considered to be useful for analyzing this transition. Fig. 6 shows the deformation and stress distribution during stage-II and stage-III creep deformation in SiC/SiC composite at 556 N applied load. The crack propagation behavior is clearly demonstrated and the stress relaxation behavior at the crack tip can be calculated also. From the definition of the interface potential, the stresses of the fiber and matrix in the interface element can be obtained. The changes in stress of the fiber and matrix along the crack path are shown in Fig. 7. After the crack propagated, both the stress of fiber and matrix decreased, and the stress of matrix became almost zero. On the other hand, the stress of fiber remained around 200 MPa after the crack propagated. In this research, as the first step for the calculation using the new method, the fiber was assumed not to fracture but to continue to creep. Although the calculated results did not exactly represent the experimental behavior, the new method is considered

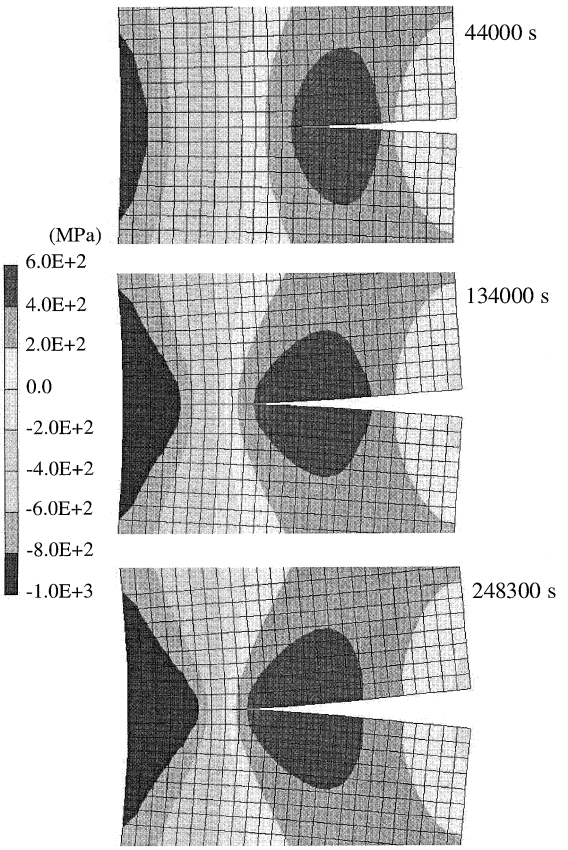

Fig. 6. Deformations and stress distributions near crack path for steady-state model.

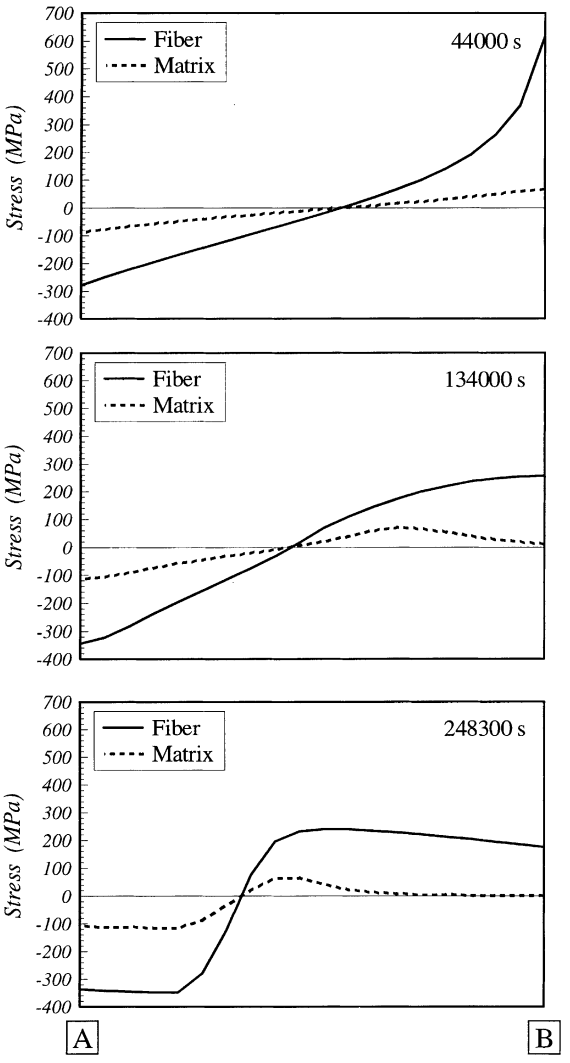

Fig. 7. Stress changes of fiber and matrix along crack path for steady-state model.

to have the potential to demonstrate the creep deformation in SiC/SiC composite. As future work, the effect of fiber fracture will be examined.

6.2. Time-dependent creep deformation (stage-I)

According to the result of previous section, the new method was applied for simulating the time-dependent creep deformation (stage-I creep deformation), which was shown in the experimental result (Fig. 3). In the case of time-dependent creep deformation, a time-dependent term must be included in the time-dependent interface element. So, in the new method, the increment of r_{f0} was defined by Eq. (10), and the parameter m and p in Eq. (10) were assumed to be 1.8 and 0.58, respectively, according to the experimental result of fiber creep test [11]. The other parameters in Eqs. (4), (5), (10) were assumed to the same as the previous analysis using the new method, where, for the parameter B , only an absolute value is same because of the difference of dimension.

Fig. 8 shows the calculated time-displacement curve of the new method with time-dependent term. Although the calculated result is very different from the experimental results in the scale, the shape of curve is parabolic as same as the experimental result. Since the difference between the steady-state model and this model in the new method is only the definition in the increment of r_{f0} , the new method is considered to have the good potential to demonstrate the creep fracture deformation in SiC/SiC composite. Fig. 9 shows the deformations and stress distributions under the computational analysis shown in Fig. 8. Only the stress relaxation behavior at the crack tip can be slightly simulated. As future works, in order to reveal the physical meanings of all parameters in Eqs. (4), (5) and (10), more simple creep deformations, which are for example a single SiC fiber creep test and a tensile creep experiment of a mini SiC/SiC composite, will be examined and simulated by using the new method.

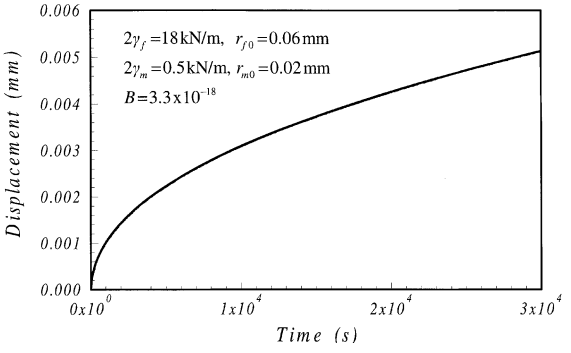

Fig. 8. Calculated displacement–time curve of new method with time-dependent term.

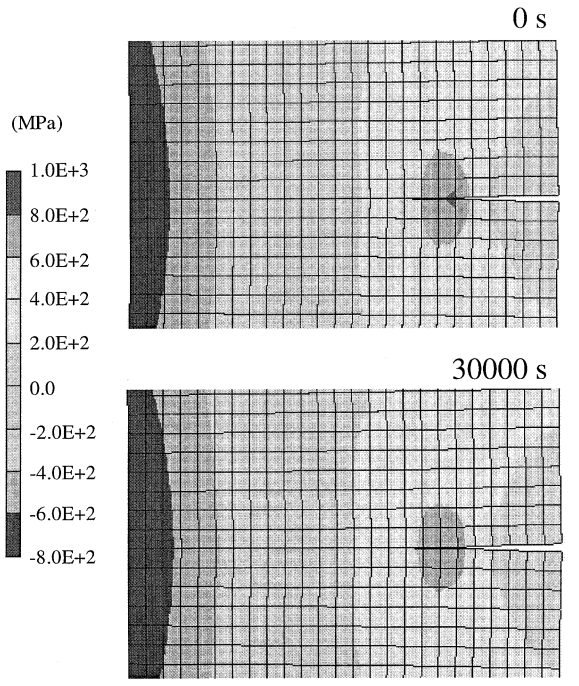

Fig. 9. Deformations and stress distributions near crack path for time dependent model.

7. Conclusions

In order to analyze creep fracture deformation in SiC/SiC composite, a new computer simulation method using time-dependent interface elements was developed and applied to crack growth deformation in SiC/SiC composites. The conclusions can be summarized as follows.

(1) Two methods were used to simulate crack growth in SiC/SiC composite due to fiber creep. In one method, the creep property was introduced into the interface elements by the general method of FEM analysis. In the second method, a new technique making the best use of the potential function was used to represent crack closure tractions due to creeping fibers. In both cases, the stage-II steady-state creep deformation was simulated.

(2) By using the new method without time-dependent term, not only the stage-III crack growth but also the transition from stage-II to stage-III could be simulated. Additionally, the parabolic curve in the stage-I creep deformation was demonstrated by the new method with time-dependent term. Therefore, the new method is considered to have the potential to model all stages of creep fracture deformation in SiC/SiC composite.

Acknowledgements

This work was maintained by Core Research for Evolutional Science and Technology: Advanced Mate-

rial Systems for Conversion of Energy. This work was also supported by Japan–US collaborative JUPITER program on fusion materials research.

References

[1] P.J. Lamicq, G.A. Bernhart, M.M. Dauchier, J.G. Mace, Am. Ceram. Soc. Bull. 65 (2) (1986) 336.
[2] J.R. Strife, J.J. Brennan, K.M. Prewo, Ceram. Eng. Sci. Proc. 11 (7&8) (1990) 871.
[3] R.H. Jones, C.H. Henager Jr., J. Nucl. Mater. 212–215 (1994) 830.
[4] R.H. Jones, C.A. Lewinsohn, G.E. Youngblood, A. Kohyama, Key Eng. Mater. 164&165 (1999) 405.
[5] C.H. Henager Jr., R.H. Jones, J. Am. Ceram. Soc. 77 (9) (1994) 2381.
[6] C.A. Lewinsohn, C.H. Henager Jr., R.H. Jones, Ceramic Trans. 74 (1996) 423.
[7] A.G. Evans, F.W. Zok, J. Mater. Sci. 29 (1994) 3857.
[8] Z.Q. Wu, H. Serizawa, H. Murakawa, Key Eng. Mater. 166 (1999) 25.
[9] H. Serizawa, H. Murakawa, Z.Q. Wu, in: Proceedings of the Eighth International Conference on Mechanical Behaviour of Materials, Vol. I, 1999, p. 261.
[10] A. Rahman, Phys. Rev. A 136 (1964) 405.
[11] J.A. DiCarlo, H.M. Yun, J.C. Goldsby, in: Proceedings of the 10th International Conference on Composite Materials, Vol. VI, 1995, p. 315.
[12] G. Boitier, J.L. Chermant, J. Vicens, Key Eng. Mater. 164&165 (1999) 317.
[13] R. Bodet, J. Lamon, N. Jia, R.E. Tressler, J. Am. Ceram. Soc. 79 (10) (1996) 2673.